



**HAL**  
open science

# Structure, age, and tectonic evolution of the Gulf of Mexico

Andreína García-Reyes, Jérôme Dymont

► **To cite this version:**

Andreína García-Reyes, Jérôme Dymont. Structure, age, and tectonic evolution of the Gulf of Mexico. *Earth and Planetary Science Letters*, 2022, 577, pp.117259. 10.1016/j.epsl.2021.117259 . insu-03452882

**HAL Id: insu-03452882**

**<https://insu.hal.science/insu-03452882>**

Submitted on 27 Nov 2021

**HAL** is a multi-disciplinary open access archive for the deposit and dissemination of scientific research documents, whether they are published or not. The documents may come from teaching and research institutions in France or abroad, or from public or private research centers.

L'archive ouverte pluridisciplinaire **HAL**, est destinée au dépôt et à la diffusion de documents scientifiques de niveau recherche, publiés ou non, émanant des établissements d'enseignement et de recherche français ou étrangers, des laboratoires publics ou privés.

1 **Structure, age, and tectonic evolution of the Gulf of Mexico**

2

3 Andreína García-Reyes and Jérôme Dyment\*

4 Université de Paris, Institut de physique du globe de Paris, CNRS, F-75005 Paris, France

5

6 \* Corresponding author: [jdy@ipgp.fr](mailto:jdy@ipgp.fr)

7

8

9 **Abstract**

10 The Gulf of Mexico is an isolated oceanic basin whose nature, structure and age are not fully  
11 elucidated, mostly because seafloor spreading isochrons have not been identified in this basin  
12 so far. We compiled and processed all publicly available marine magnetic data to produce a  
13 new magnetic anomaly map of the Gulf of Mexico. This map reveals a fan-like set of  
14 intermediate-wavelength (>100 km) magnetic anomalies related to seafloor spreading. Our  
15 magnetic anomaly-based plate reconstructions (1) support a counterclockwise rotation of the  
16 Yucatán Block around a pole located NW of Cuba, (2) accommodate the fracture zone trends  
17 depicted by the gravity data, and (3) suggest that the Continent-Ocean Boundary lies  
18 immediately south of the Houston magnetic anomaly, close to the shoreline, implying that  
19 oceanic crust underlies a significant part of the Sigsbee salt province. Our attempt to identify  
20 the intermediate wavelength anomalies by comparison with filtered Geomagnetic Polarity  
21 Time Scales dates the onset of seafloor spreading before the Tithonian (>150 Ma) and its  
22 cessation at the Berriasian (140 Ma).

23

24

25 **Introduction**

26 Most authors agree on the presence of oceanic crust within the Gulf of Mexico (hereafter  
27 GoM), the location of the transition between oceanic and continental crust remains  
28 controversial (e.g., [Eagles et al., 2015](#)). The kinematics of this isolated basin is crucial to  
29 understand the tectonic evolution of America during the breakup of Pangea. As one of the  
30 richest petroleum provinces of the world, it has been explored intensively for several decades  
31 and imaged by countless seismic data. More recently, satellite-derived vertical gradient of  
32 gravity (VGG) illuminated fracture zones in its western part ([Bonvalot et al., 2012](#); [Sandwell  
33 et al., 2014](#)). Gravity data interpretation remain unclear in some areas, preventing the  
34 structure (and therefore the nature – oceanic or continental) of the crust to be unraveled. This  
35 is the case in the northern GoM, where the gravity signal of thick salt and sediment deposits  
36 overprint that of the underlying crust. Based on the Jurassic age (Bajocian to Oxfordian) of  
37 this salt ([Pindell et al., 2020](#)) and the Late Jurassic-Cretaceous age of later sediments (e.g.,  
38 [Galloway, 2008](#); [Snedden et al., 2015](#); [Lin et al., 2019](#)), previous evolution models  
39 considered that the GoM started to open during the Jurassic ([Carey, 1958](#); [Bullard et al.,  
40 1965](#); [Pindell and Dewey, 1982](#); [Hall et al., 1982](#); [Schlager et al., 1984](#), [Buffler and Sawyer,  
41 1985](#); [Ross and Scotese, 1988](#); [Keppie and Keppie, 2014](#)). The counter-clockwise rotation of  
42 the Yucatán Block (e.g., [Pindell and Dewey, 1982](#); [Marton and Buffer, 1994](#)) is confirmed by  
43 paleomagnetic results (e.g., [Molina-Garza et al., 1992](#)). Such an opening would be  
44 contemporaneous to that of the nearby Central Atlantic ([Marzoli et al., 1999](#); [Blackburn et al.,  
45 2013](#)). However, despite an abundant data set, marine magnetic anomalies related to seafloor  
46 spreading– which would provide the structure, the age, and therefore the evolution of the  
47 GoM – remain elusive and debatable. Several authors (e.g., [Nguyen et al., 2015](#); [Pindell et  
48 al., 2016](#); [Lundin and Doré, 2017](#); [Lin et al., 2019](#); [Minguez et al., 2020](#)) followed the VGG  
49 interpretation of [Sandwell et al. \(2014\)](#) to locate the GoM fossil spreading center, transform

50 faults, and continent-ocean boundary (COB). They present excerpts of the available global  
51 magnetic anomaly maps but failed to recognize a regional magnetic anomaly pattern  
52 supporting their interpretation.

53 In this paper, we present a new geophysical interpretation of the GoM based primarily on  
54 marine magnetic anomaly data. The major differences between our and previous works can  
55 be summarized in five points:

56 (1) We compiled, processed and reassessed all the available marine magnetic data in the  
57 GoM. As a result, we derived a new, improved magnetic anomaly map of the GoM. This  
58 important effort allowed us to observe a symmetrical pattern of intermediate-wavelength  
59 magnetic anomalies that we ascribe to seafloor spreading in the basin.

60 (2) The location of the (main) fossil spreading center is primarily based on the  
61 interpretation of the new magnetic anomaly map and corresponds to the symmetry  
62 axis of the conjugate magnetic anomalies of the basin. This location differs from those  
63 from previous studies (Supplementary Figure S6). Although we agree with the  
64 interpretation of [Sandwell et al. \(2014\)](#) for the transform faults and fracture zones, we  
65 consider their two short segments of abandoned spreading axis in the southwestern  
66 GoM as reflecting local ridge jumps further substantiated by the spreading asymmetry  
67 seen from the magnetic anomaly interpretation. Conversely, the western part of the  
68 main fossil spreading axis constrained by the magnetic anomalies bears no VGG  
69 signature, because it is buried beneath the southern Sigsbee Salt Province and its  
70 gravity signature is hidden amongst the gravity signals of complex structures related  
71 to salt tectonics and/or sedimentation history.

72 (3) Unlike previous studies, we mostly use our new magnetic anomaly map (with the  
73 truncation of continental anomalies and presence of seafloor spreading anomalies),  
74 complemented by the VGG (with the shelf-break), to define the location of the COB in

75 the study area. The location of our COB significantly differs from many previous  
76 interpretations in the northwestern GoM, off Texas and Louisiana. These previous  
77 interpretations cannot be reconciled with the observed magnetic anomalies.

78 (4) We attempt to date the observed magnetic anomalies by comparison with a filtered  
79 geomagnetic polarity time scale. Although not a classical approach, the lack of short  
80 wavelength magnetic anomalies on the available data offers no better option.

81 (5) As a consequence of these different interpretations, we present a new, consistent model  
82 for the opening of the GoM based on the new magnetic anomaly map.

83

#### 84 **Data and methods**

##### 85 *Building the Magnetic Map of the Gulf of Mexico*

86 We processed total marine magnetic field measurements and combined them to obtain a new  
87 magnetic anomaly map at a grid interval of 3 km (Figure 1a). We recovered the total  
88 magnetic field measurements from the data repositories of the National Center for  
89 Environmental Information (NCEI) (formerly the National Geophysical Data Center)  
90 (Supplementary Figure S1) The magnetic pre-processing included removing spurious data,  
91 excluding noisy tracks and performing quality control over navigation and acquisition time  
92 along marine tracks (Supplementary Figure S2). We calculated magnetic anomalies by  
93 removing models of the Earth's internal magnetic field. To this end, we used the  
94 Comprehensive Magnetic Model v.4 (CM4; Sabaka, 2004) for the time interval between 1960  
95 and 2002.5, complemented by the IGRF-11 (Thébault et al., 2015) for data acquired outside  
96 this time range. We performed internal and external leveling of the marine tracks to reduce  
97 the misfit at the crossovers (see details in García-Reyes, 2018; Supplementary Table S1). We  
98 complemented the map built with marine data with the WDMAM v. 2.0 (Lesur et al., 2016)  
99 on land. We applied different filters in an attempt to unravel possible magnetic anomalies

100 related to seafloor spreading (Supplementary Figure S3). Applying a Gaussian filter to keep  
101 wavelengths > 100 km removed spurious effects from local short wavelength anomalies and  
102 artefacts and retains what we regard as the reliable spectral content. The resulting map  
103 (hereafter named "intermediate wavelength magnetic anomaly map") is used in all  
104 interpretations of this paper.

105 Although using reduced-to-the pole (RTP) magnetic anomalies, which unambiguously lie  
106 above their causative sources, would make interpretations and comparisons easier, we have  
107 no clear indication whether these anomalies are caused by induced or by remanent  
108 magnetization. In the latter case, computing RTP anomalies would require the direction of the  
109 remanent magnetization vector to be reliable. Because we lack constraints on this parameter,  
110 we preferred not to compute a RTP magnetic anomaly.

111

### 112 *From potential field data to plate motion model*

113 We inspected the pattern of the available gravity and marine magnetic data to identify  
114 seafloor spreading features and the Continent-Ocean Boundary (COB) in the GoM. We  
115 interpreted the magnetic anomalies and built a tectonic map of the basin by recognizing  
116 conjugate anomalies with respect to a central magnetic anomaly that marks the extinct ridge  
117 axis (Figure 1b). We used each pair of conjugate magnetic isochrons to calculate finite  
118 rotations (pole and angle of rotation, Supplementary Table S2), from which we derived stage  
119 rotations. We then constructed our plate evolution model for the opening of the GoM (Figure  
120 2). We tried to account for both the interpreted magnetic anomalies and the fracture zones  
121 observed on VGG (Figure 1).

122 Since only intermediate wavelength magnetic anomalies related to seafloor spreading could  
123 be recognized, we lack precise isochrons determinations and cannot use the statistical method  
124 of [Chang \(1988\)](#) for computing the finite rotation parameters. Instead, we approximated the

125 interpreted fracture zones with small circles, determined great circles perpendicular to those  
126 modelled fracture zones (simulating the projection of the rotation axis on a spherical shape),  
127 and employed a best-fitting method to determine crossings of the great circles, i.e. possible  
128 Euler poles (Morgan, 1968). We considered crossings as trial poles and kept those ones with  
129 the higher statistical count. We produced flowlines with the selected poles, building segments  
130 of small circles for each stage rotation poles, and compared them with the interpreted fracture  
131 zones for validation (Figure 3; Supplementary Figure S5). We qualitatively compared  
132 different sets of flowlines (built with different sets of rotation poles) with the interpreted FZs.  
133 The COB shows a major contrast of density and magnetic properties in the crust and the  
134 lithosphere. Therefore, we infer that it is located within a relatively narrow zone of high  
135 gravity and magnetic gradients in the south and east of the GoM. Although they may not be  
136 isochrons *sensu stricto*, we reconstructed the conjugate COBs to determine rotation  
137 parameters for the total closure of the GoM (Supplementary Table S2 and Supplementary  
138 Figure S7).

139

#### 140 *Age and Spreading rate*

141 We vainly tried to analyze the few well-oriented individual magnetic profiles for profile-to-  
142 profile similarities and similarities to synthetic magnetic anomaly models. We therefore  
143 confirm that the amount, resolution and quality of the available magnetic data in the GoM is  
144 insufficient to attempt a detailed identification of marine magnetic anomalies within the  
145 whole basin. Although this point needs additional data to be conclusively sorted out, we  
146 suspect that short wavelength magnetic anomalies related to seafloor spreading may be absent  
147 in the GoM for reasons that are developed below.

148

149 We therefore attempted to date the seafloor by comparing the observed intermediate  
150 wavelength anomalies to various filtered Geomagnetic Polarity Time Scales (GPTS). In order  
151 to match the wavelength of the observed magnetic anomalies, each GPTS was filtered using  
152 various Gaussian filters to account for a range of different possible spreading rates  
153 (Supplementary Figure S11). The filtered polarity time scales were compared to five  
154 magnetic profiles extracted from the intermediate wavelength magnetic anomaly map (see  
155 above) along flowlines to attempt identifying the magnetic isochrons (Figure 4). Different  
156 possible solutions were considered with respect to the available geological data and the most  
157 geologically reasonable interpretation was selected, from which ages were ascribed to the  
158 anomalies (Supplementary Table S5; Supplementary Figure S13). This exercise implicitly  
159 assumes that no major change of angular velocities occurred during the opening of the basin.  
160 We calculated spreading rate and asymmetry along each flowline (Supplementary Tables S3  
161 and S4; Supplementary Figures S9 and S10).

162

### 163 **A New Magnetic Map of the Gulf of Mexico**

164 Unlike most of the previous magnetic maps for the area (e.g., [Bankey et al., 2002](#)) but in  
165 agreement with a recent dense aeromagnetic map of the southern GoM ([Pindell et al., 2016](#)),  
166 our new magnetic anomaly map displays a group of East-West elongated intermediate  
167 wavelength and low amplitude (-50 - +50 nT) anomalies. The group is made of three positive  
168 and four negative anomalies. The central positive anomaly is the longest one and extends  
169 over ~1500 km, whereas the outer positive anomalies are ~1000 km long. The anomalies on  
170 both sides of the central one appear to be symmetrical at first order, with similar lateral  
171 variations in extent, width, and amplitude. Altogether they define a magnetic fan-like  
172 structure that we consider reflects the seafloor spreading evolution of the GoM. Aside from  
173 this oceanic domain we identify four distinct magnetic domains surrounding the GoM: the

174 conjugate Yucatán (1, see Supplementary Figure S7) and Florida (2) cratonic blocks show  
175 strong anomalies of relatively long wavelength that a proper reconstruction aligns,  
176 emphasizing their pre-rift origin, only locally erased by the later Chicxulub impact at 65 Ma.  
177 The Trans Mexican volcanic belt (3) exhibits moderate amplitude and shorter wavelength  
178 anomalies. The basins fringing Louisiana and Texas, the Western Gulf Coast Basin and the  
179 Texas-Louisiana-Mississippi Salt Basin (4) display an East-West elongated positive magnetic  
180 anomaly that was interpreted as intracontinental by previous workers (Houston magnetic  
181 anomaly, after [Hall et al., 1990](#)).

182

### 183 **The Continent-Ocean Boundary**

184 The free-air gravity anomaly and its vertical gradient often display a sharp signal at the shelf-  
185 break, which sometimes corresponds to the COB but may also be shifted oceanward  
186 depending on the pattern of sediment accumulation and possible underplating or post-rift  
187 magmatism. The magnetic anomaly is also not always conclusive, the COB being sometimes  
188 - but not systematically - marked by a magnetic anomaly corresponding to synrift volcanic  
189 activity. South and Northeast of the GoM (domains 1 and 2), we inferred the COB from both  
190 the sharp gradients of magnetic anomalies and vertical gradients of gravity, which show a  
191 good agreement (Figure 1). This inference is supported by seismic data (e.g., [Christeson et](#)  
192 [al., 2014](#)). In the western GoM, the signature of fracture zones in gravity data confirms the  
193 oceanic nature of its crust ([Sandwell et al., 2014](#), Figure 1c and d). In this area (domain 3),  
194 we interpret the Eastern Mexico Transform Margin (also known as Tamaulipas-Golden Lane-  
195 Chiapas Transform) as the COB, as proposed by previous authors (e.g., [Nguyen et al., 2015](#)).  
196 The location of the COB in the north-western and north-central parts of the GoM (domain 4)  
197 has been more widely discussed due to the ambiguous signature of their potential field and  
198 seismic data. The gravity signal of the underlying crust is obscured by the thick sediments

199 (including evaporites) of the Sigsbee salt province (Supplementary Figure S4). Seismic  
200 reflection and refraction data there suggest a progressive thinning of the crust oceanward  
201 (e.g., Profiles GUMBO 1 off Texas; [Van Avendonk et al., 2015](#); and GUMBO 2 off  
202 Louisiana; [Eddy et al., 2018](#)) without a sharp transition that might unambiguously be  
203 interpreted as the COB, as in the eastern GoM (e.g., Profile GUMBO 3 off Alabama; [Eddy et](#)  
204 [al., 2014](#); and GUMBO 4 off Florida; [Christeson et al., 2014](#)). Our interpretation of the COB  
205 does therefore not contradict the GUMBO seismic data. Conversely, the symmetry of the fan-  
206 like anomalies in the GoM oceanic domain requires the COB in domain 4 to lie immediately  
207 south of the Houston magnetic anomaly, close to the shoreline. As a consequence, the  
208 northernmost anomaly related to seafloor spreading is found ~300 km north of the southern  
209 boundary of the Sigsbee salt province, implying that oceanic crust underlies a significant part  
210 of this province.

211 We confirmed the location of the COB in the controversial areas by attempting to juxtapose  
212 the conjugate COB and close the GoM (Supplementary Figure S7). This is not a plate  
213 reconstruction *sensu stricto*, as the COB is not necessarily an isochron. The observed fan-like  
214 shape of the magnetic anomalies implies that the pole of the Euler rotation closing the GoM  
215 lies NW of Cuba, immediately south of Florida and east of Yucatán, as suggested by previous  
216 studies (e.g., [Pindell, 1985](#); [Bird and Burke, 2006](#); among others). We achieved the closure of  
217 the GoM by juxtaposing the conjugate COBs where they are both well constrained, off the  
218 North Coast of Yucatán and the West Coast of Florida, respectively. The best-fitting rotation  
219 has a pole at 85.18°W, 23.99°N and an angle of 59° (geocentric latitude). Magnetics show a  
220 good correspondence between reconstructed Yucatán and Florida, with continuous magnetic  
221 anomalies across the margin (Supplementary figure S7). Further West, the Houston magnetic  
222 anomaly and a strong parallel magnetic high on the Yucatán Block may mark early  
223 magmatism on the passive margin.

224

## 225 **The Oceanic Basin**

226 In this section, we focus on the oceanic basin to further investigate the GoM plate tectonic  
227 history. The tectonic features available to attempt plate reconstructions are (1) the COB as  
228 previously defined from gravity and magnetics; (2) the few fracture zones identified on the  
229 VGG in the west GoM (Sandwell et al., 2014); and (3) conjugate magnetic anomalies.

230 We identified pairs of conjugate anomalies and the fossil ridge axis within the fan-like  
231 structure observed on the magnetic anomaly map (Figures 1 and 3). The axis of symmetry is  
232 a positive anomaly, marked GoM1, that extends from East to West along the whole oceanic  
233 basin and marks the fossil spreading center. It is flanked on each side by a pair of roughly  
234 symmetrical positive anomalies marked GoM2. These anomalies are observed off the  
235 Mexican Coast in the Western GoM and abut the COB off Florida at  $\sim 87^\circ\text{W}$  and off Yucatán  
236 at  $\sim 89^\circ\text{W}$ . It is worth noting that conjugate anomalies abut conjugate parts of the COB. The  
237 truncation of the older anomalies to the East suggests that the seafloor spreading propagated  
238 from West to East in this area, in relation to the progressively slower relative plate motion  
239 toward the rotation pole.

240 The conjugate magnetic anomalies constrain the detailed plate tectonic evolution of the GoM.  
241 The GoM1 and GoM2 positive anomalies offer three isochrons, namely the older side of  
242 GoM1 (GoM1o) and the younger and older sides of GoM2 (GoM2y and GoM2o,  
243 respectively), to attempt plate reconstructions. However, the GoM1o isochrons are too close  
244 to each other to provide any meaningful results. We therefore limit our magnetic  
245 reconstructions to GoM2y and GoM2o. Unlike classical plate reconstructions based on  
246 individual magnetic anomaly identification on individual profiles, our isochrons are  
247 interpreted from intermediate wavelength anomalies on gridded data. Therefore, instead of  
248 attempting to use the whole isochrons, we preferred to match specific features recognized on

249 both conjugate isochrons such as fracture zone offsets to compute the rotation parameters  
250 (Figure 3). The resulting plate reconstructions are shown in Figure 2.

251 We computed stage rotations on both flanks for the GoM2o-GoM2y interval from the finite  
252 rotations reconstructing conjugate anomalies GoM2y and GoM2o, respectively. The finite  
253 and stage poles all lie between Yucatán and Florida (Figure 3). Finite and stage rotation  
254 parameters are given in Supplementary Table S2. The flow lines built from the resulting  
255 model are in reasonable agreement with the fracture zone trend observed on the VGG in the  
256 western GoM (Figure 3; Supplementary Figure S5) and describes the seafloor spreading  
257 evolution of the GoM after the age of anomaly GoM2o.

258 The eastwards truncation of magnetic anomaly GoM2 at the COB confirms that the COB is  
259 not an isochron. Therefore, the total closure reconstruction should only be regarded as an  
260 exercise to evaluate the respective initial location of the two continental blocks and the  
261 continuity of gravity and magnetic features across their passive margins. Clearly, these  
262 margins experienced stretching and deformation when seafloor spreading was already  
263 occurring to the west, and therefore an accurate initial reconstruction should take this  
264 deformation into account, which is out of the scope of this paper. As a consequence, our total  
265 closure rotation parameters do not predict a spreading direction compatible with the observed  
266 fracture zones in the Western GoM (Supplementary Figure S8).

267 Two distinct tectonic phases are therefore recognized for the opening of the GoM. In the first  
268 phase, the western part of the Gulf was experiencing seafloor spreading whereas the eastern  
269 part was still under continental rifting. The breakup progressively propagated eastward. No  
270 meaningful reconstruction parameters could be derived for this phase due to the lack of  
271 appropriate isochrons. The second phase started once breakup was achieved along most of the  
272 basin, at the age of GoM2o. A steadier regime of seafloor spreading established, in which the  
273 available isochrons allow us to distinguish two sets of stage rotation parameters for GoM2o-

274 GoM2y and GoM2y-GoM1y. These rotation poles are closely bunched together and would  
275 probably be statistically indistinguishable if statistical plate reconstruction methods could be  
276 applied in the GoM.

277

### 278 **Dating the intermediate-wavelength magnetic anomalies**

279 Our plate tectonic model for the evolution of the GoM still lacks an essential aspect: neither  
280 the onset of seafloor spreading nor isochrons GoM2 and GoM1 have been ascribed an age so  
281 far. For reasons that are either related to the data distribution and quality, or to the processes  
282 of oceanic crust emplacement in young, isolated basins with thick sediments and evaporites  
283 (e.g., [Dyment et al., 2013](#); see below), the classical short-wavelength magnetic anomalies  
284 associated to seafloor spreading could not be recognized in the GoM. We compare the  
285 sequence of observed intermediate wavelength anomalies with filtered GPTS in an attempt to  
286 recognize and therefore date these anomalies. Five representative profiles were extracted  
287 from the anomaly map following flowlines defined by the rotation parameters. Considering  
288 the uncertainties on the M-series GPTS, we carried out the same procedure on four published  
289 GPTS ([Kent and Gradstein, 1986](#); [Gradstein and Ogg, 1996](#); [Tominaga and Sager, 2010](#);  
290 [Malinverno et al., 2012](#), used in Figure 4) to ensure that the result does not depend on  
291 peculiarities of a given time scale (Supplementary Figure S11).

292 Global plate reconstructions and apparent polar wander models suggest that the GoM opened  
293 at about 20°N ([van Hinsbergen et al., 2015](#)). Assuming that it was formed at the Equator  
294 along an approximately E-W spreading center and observed at the same location predicts  
295 magnetic anomalies centered on their causative source with normal polarity generating a  
296 negative anomaly and reversed polarity a positive anomaly (i.e., skewness = 180°). We first  
297 adopt these simplifying assumptions and, to take into account this effect, we inverted the  
298 filtered GPTS before attempting to identify the observed intermediate wavelength anomalies.

299 We discuss the effect of more realistic paleo- and present latitudes and spreading center  
300 directions in Supplementary Figure S12. Although the skewness of the observed intermediate  
301 wavelength magnetic anomalies remains an elusive parameter, adopting more realistic  
302 assumptions does not affect our interpretation but results in a 50 to 100 km shift of the fossil  
303 spreading center and isochrons southward.

304 Our best fit between the inverted filtered GPTS and the observed profile, obtained for all  
305 tested GPTSs, identifies the high of intermediate magnetic anomaly GoM1 with Chron M17r  
306 and the high of GoM2 with Chrons M22r and M23r (Figure 4; Supplementary Figure S13).

307 We acknowledge that other acceptable solutions with different spreading rates and ages may  
308 be obtained but consider this solution to be the most geologically plausible, both for the  
309 predicted spreading rates and the age of seafloor spreading onset and demise. If correct, this  
310 model predicts the onset of seafloor spreading in the GoM before the Tithonian and the  
311 cessation of seafloor spreading at the end of the Berriasian. These ages are consistent with  
312 geological studies of both conjugate margins (e.g., [Stern and Dickinson, 2010](#); [Barboza-](#)  
313 [Gudino et al., 2012](#); [Marton and Buffler, 2016](#)). The analysis of seismic profiles linking  
314 stratigraphy from wells on the Florida platform to the fossil spreading center in the Eastern  
315 GoM confirms the Berriasian age of the spreading cessation ([Lin et al., 2019](#)).

316

## 317 **Discussion**

### 318 - *Proximity of the rotation pole*

319 The finite and stage rotation poles that describe the relative plate motions for the origin of the  
320 GoM are all located in the close vicinity of the eastern tip of the oceanic basin, as suggested  
321 by the fan-like shape of the observed magnetic anomalies and in agreement with previous  
322 studies (e.g., [Pindell et al., 1985](#); [Bird and Burke, 2006](#); among others). Spreading rates  
323 therefore increase rapidly westward across the basin. On average, they vary from less than 20

324 km/Myr in the East to about 50 km/Myr in the West, i.e. from slow (and probably ultraslow  
325 in the easternmost tip of the oceanic basin) to fast spreading (Supplementary Figure 9 and  
326 Supplementary Table 3). The magnetic anomaly model presented in Figure 4 is valid for the  
327 fast to slow spreading rates of the Western and Central GoM, but it may not be suitable for  
328 the Easternmost GoM, where ultraslow spreading rates are expected and more drastic filters  
329 would have to be applied to the GPTS to adequately model the observed anomalies. The  
330 interpretation of marine magnetic anomalies in ultraslow spreading areas is a difficult  
331 exercise and the available data do not allow further elaboration on this matter.

332

### 333 - *Asymmetry and abandoned spreading segments*

334 A more detailed appraisal of the magnetic anomaly map reveals spreading asymmetry in the  
335 basin. Two maps and tables are presented, showing the total asymmetry (Supplementary  
336 Figure 10a and Supplementary Table S4) and the stage by stage asymmetry (Supplementary  
337 Figure 10b and Supplementary Table S4). The stage by stage asymmetry shows quite a large  
338 scatter with no systematic trends, especially for the shorter GoM2o-GoM2y stage. This  
339 reflects the increasing relative weight of the uncertainties on the isochron location with  
340 respect to the stage duration. Conversely, the total symmetry shows four distinct corridors  
341 with systematic asymmetry. Flowlines 1-2 show asymmetry to the benefit of the northern  
342 flank (corridor A), flowlines 5-10 of the southern flank (corridor B), flowlines 13-14 of the  
343 northern flank (corridor C), and flowlines 17-19 of the southern flank (corridor D). The effect  
344 of this asymmetry is to progressively reshape the ridge axis, as the arc-shape described by the  
345 COBs in the Western and Central GoM progressively evolved to the more sinuous fossil  
346 ridge axis. The strongest asymmetry, more than 60%, is observed in corridor B and is most  
347 probably accommodated by ridge jumps, explaining the two short segments of abandoned  
348 spreading axis left on the southern flank in the Western GoM and identified on the VGG

349 (Sandwell et al., 2014; red lines on Figure 1d and Supplementary Figure S5). These segments  
350 lie in an anomalously wide magnetic anomaly which reflects a northward ridge jump and the  
351 abandonment of a fossil axis on the southern flank.

352

353 - *Why are short wavelength magnetic anomalies not observed in the GoM?*

354 The reason why short-wavelength magnetic anomalies have not been depicted in the GoM so  
355 far is still uncertain. The paucity of marine data and/or their inadequacy to define lineated  
356 short-wavelength anomalies may be a reason. However, proprietary aeromagnetic surveys  
357 exist over parts of the GoM (e.g., Pindell et al., 2016). We suspect that the 3 km-interval (EW  
358 lines) and 9 km-interval (NS lines) of the proprietary aeromagnetic survey flown some 15 km  
359 or less above the basement (Pindell et al., 2016) would have allowed the depiction of  
360 anomalies of wavelength shorter than 100 km if such anomalies existed. However, we cannot  
361 exclude that the aeromagnetic map published by Pindell et al. (2016) was degraded to a lower  
362 resolution for the purpose of publication, although this is not mentioned in the paper.

363 The other possibility is that such short wavelength anomalies do not actually exist. Two  
364 scenarios may explain their absence. In the first one, abundant post-accretion sedimentation  
365 may have erased the magnetic anomalies due to the extrusive basalt titanomagnetite (Curie  
366 temperature ~200°C) by reheating and partial thermal demagnetization, as suggested by Levi  
367 and Riddihough. (1986) for the Gulf of California, the Gulf of Aden, and the northern Red  
368 Sea, and by Granot and Dymant (2019) for the South Atlantic margin off Argentina. In the  
369 second one, abundant syn-accretion sedimentation – and the presence of mobile evaporitic  
370 deposits – would have inhibited the formation of the extrusive basalt layer, replaced by  
371 intrusive (and therefore less magnetic) sills, as suggested by Dymant et al. (2013) for most of  
372 the Red Sea. In both instances, the observed intermediate-wavelength magnetic anomalies are

373 caused by the deeper crustal layers whose magnetic mineral, magnetite, has a higher Curie  
374 temperature (~580°C).

375 Solving this pending issue requires access to the existing dense aeromagnetic surveys over  
376 the GoM and/or the acquisition of new marine magnetic anomaly profiles along flowlines.

377

### 378 **Conclusion**

379 Our compilation and processing of marine magnetic anomalies allowed us to identify  
380 intermediate-wavelength magnetic anomalies related to seafloor spreading in the Gulf of  
381 Mexico (GoM). We identified the fossil ridge axis and a pair of conjugate positive anomalies  
382 and deciphered the GoM plate tectonic history from the magnetic isochrons, fracture zones as  
383 imaged by gravity, and the COB depicted from both gravity and magnetics. The fan-shape  
384 structure of the observed magnetic anomalies supports a counterclockwise rotation of the  
385 Yucatán Block with respect to a pole located NW of Cuba. The older magnetic anomalies  
386 abut on the COB, suggesting that oceanization propagated from West to East. The  
387 observation of seafloor spreading magnetic anomalies on the offshore part of the Sigsbee Salt  
388 Province implies that it is underlain by oceanic crust, as is the offshore part of the Campeche  
389 Salt Province. Our plate reconstruction model suggests two stages of evolution: the first one  
390 showed continental rifting in the East and seafloor spreading in the West, the latter  
391 propagating eastward at the expenses of the former; and the second one, after completion of  
392 the breakup, showing seafloor spreading along the entire GoM. Filtering the geomagnetic  
393 polarity time scale allowed us to tentatively date the observed anomalies (and therefore the  
394 second stage): seafloor spreading onset in the GoM predates the Tithonian (>150 Ma) and  
395 stopped during the Berriasian (140 Ma). As reflected by the proximity of the rotation poles,  
396 strong spreading rate variations are observed from ultraslow in the easternmost GoM to fast

397 in the West, where the measured spreading asymmetry confirms our interpretation of short,  
398 abandoned spreading segments.

399

400 **Data availability.** We downloaded marine total magnetic field measurements from the  
401 National Center for Environmental Information (formerly National Geophysical Data Center;  
402 [www.ngdc.noaa.gov/mgg/geodas/trackline.html](http://www.ngdc.noaa.gov/mgg/geodas/trackline.html)). Magnetic anomalies on land are from the  
403 World Digital Magnetic Anomaly Map (Dyment et al., 2015; Lesur et al., 2016; [wdmam.org](http://wdmam.org)).  
404 Vertical gradients of gravity are available from the Scripps Institution of Oceanography,  
405 University of California in San Diego (Sandwell et al., 2014; [topex.ucsd.edu](http://topex.ucsd.edu)). A low-  
406 resolution version of the magnetic anomalies supporting the findings of this study will be  
407 incorporated in the WDMAM version 2.1. The full resolution version is available from the  
408 corresponding author upon request.

409

410 **Acknowledgements.**

411 AGR has been supported by a PhD scholarship of Fundayacucho and Campus France and  
412 additional support from IPGP, as well as a Postdoctoral Fellowship of Programme PAUSE.  
413 We thank all scientists and crews who collected the marine geophysical data used in this  
414 study. This is IPGP contribution xxx.

415

416 **References**

- 417 1. Bankey, V., Cuevas, A., Daniels, D., Finn, C. A., Hernandez, I., Hill, P., Kucks, R.,  
418 Miles, W., Pilkington, M., Roberts, C., Roest, W., Rystrom, W., Shearer, S., Snyder,  
419 S., Sweeney, R., Velez, J., Philips, J.D., Ravat, D. (2002). Digital data grids for the  
420 magnetic anomaly map of North America. U.S. Geological Survey Open-File Report  
421 02-414, U.S. Geological Survey Denver Colorado USA.
- 422 2. Barboza-Gudino, J.R., R.S. Molina-Garza, and T.E. Lawton (2012). Sierra de  
423 Catorce: Remnants of the ancient western equatorial margin of Pangea in central  
424 Mexico, in J.J. Aranda-Górner, G. Tolsan, and R.S. Molina-Gana, eds., *The Southern  
425 Cordillera and Beyond: Geological Society of America Field Guide 25*. p. 1–18,  
426 [https://doi.org/10.1130/2012.0025\(01\)](https://doi.org/10.1130/2012.0025(01)).
- 427 3. Bird, D., and Burke, K. (2006). Pangea breakup: Mexico, Gulf of Mexico, and Central  
428 Atlantic Ocean. SEG Technical Program Expanded Abstracts, 1013-1017a,  
429 <https://doi.org/10.1190/1.2369685>.
- 430 4. Blackburn, T. J., Olsen, P. E., Bowring, S. A., McLean, N. M., Kent, D. V., Puffer, J.,  
431 McHone, G., Rasbury, E. T., and Et-Touhami, M. (2013). Zircon U-Pb  
432 geochronology links the end-Triassic extinction with the Central Atlantic Magmatic  
433 Province. *Science*, 340(6135):941–945, <https://doi.org/10.1126/science.1234204>.
- 434 5. Bonvalot, S., Balmino, G., Briais, A., Kuhn, M., Peyrefitte, A., Vales, N., Biancale,  
435 R., Gabalda, G., Moreaux, G., and Reinquin, F. (2012). World Gravity Map,  
436 1:50000000 (map). BGI-CGMW-CNES-IRD, <https://doi.org/s00190-011-0533-4>.
- 437 6. Buffler, R. T., and Sawyer, D. S. (1985). Distribution of crust and early history, Gulf  
438 of Mexico basin. *Gulf Coast Association of Geological Societies Transactions*,  
439 35:333–344, <https://doi.org/10.1306/AD462C9F-16F7-11D7-8645000102C1865D>.

- 440 7. Bullard, E., Everett, J. E., and Smith, A. G. (1965). The fit of the continents around  
441 the Atlantic. *Phil. Trans. R. Soc. Lond. A*, 258(1088):41–51,  
442 <https://doi.org/10.1098/rsta.1965.0020>.
- 443 8. Carey, S. W. (1958). Continental Drift, a Symposium: Being a Symposium on the  
444 Present Status of the Continental Drift Hypothesis. Held in the Geology Department  
445 of the University of Tasmania in March, 1956, volume 2. Geology Department,  
446 University of Tasmania.
- 447 9. Chang, T. (1988). Estimating the relative rotation of two tectonic plates from  
448 boundary crossings. *Journal of the American Statistical Association*, 83(404):1178-  
449 1183, <https://doi.org/10.1080/01621459.1988.10478717>.
- 450 10. Christeson, G., Van Avendonk, H., Norton, I., Snedden, J., Eddy, D., Karner, G., and  
451 Johnson, C. (2014). Deep crustal structure in the eastern Gulf of Mexico. *Journal of*  
452 *Geophysical Research: Solid Earth*, 119(9):6782–6801,  
453 <https://doi.org/10.1002/2014JB011045>.
- 454 11. Dymant, J., Tapponnier, P., Afifi, A. M., Zinger, M. A., Franken, D., and Muzaiyen,  
455 E. (2013). A new seafloor spreading model of the Red Sea: magnetic anomalies and  
456 plate kinematics. Abstract T21A-2512 presented at 2013, Fall Meeting, AGU, San  
457 Francisco, CA, 9-13 December.
- 458 12. Dymant, J., Choi, Y., Hamoudi, M., Lesur, V., and Thébault, E. (2015). Global  
459 equivalent magnetization of the oceanic lithosphere. *Earth and Planetary Science*  
460 *Letters*, 430:54-65, <https://doi.org/10.1016/j.epsl.2015.08.002>.
- 461 13. Eagles, G., Pérez-Díaz, L., Scarselli, N. (2015). Getting over continent ocean  
462 boundaries. *Earth-Science Reviews*, 151:244-265, ISSN 0012-8252,  
463 <https://doi.org/10.1016/j.earscirev.2015.10.009>.

- 464 14. Eddy, D. R., Van Avendonk, H. J. A., Christeson, G. L., Norton, I. O., Karner, G. D.,  
465 Johnson, C. A., and Snedden, J. W. (2014). Deep crustal structure of the northeastern  
466 Gulf of Mexico: Implications for rift evolution and seafloor spreading, *J. Geophys.*  
467 *Res. Solid Earth*, 119: 6802– 6822, <https://doi:10.1002/2014JB011311>.
- 468 15. Eddy, D. R., Van Avendonk, H. J., Christeson, G. L., and Norton, I. O. (2018).  
469 Structure and origin of the rifted margin of the northern Gulf of Mexico. *Geosphere*,  
470 14 (4):1804-1817, <https://doi.org/10.1130/GES01662.1>.
- 471 16. Galloway, W. (2008). Chapter 15 Depositional Evolution of the Gulf of Mexico  
472 Sedimentary Basin. Editor(s): Andrew D. Miall, *Sedimentary Basins of the World*,  
473 Elsevier, 5:505-549, ISSN 1874-5997, ISBN 9780444504258,  
474 [https://doi.org/10.1016/S1874-5997\(08\)00015-4](https://doi.org/10.1016/S1874-5997(08)00015-4). García-Reyes, A. (2018). Magnetic  
475 anomalies and plate tectonic history of the Caribbean plate and the Gulf of Mexico  
476 (Doctoral dissertation, Université Sorbonne Paris Cité). [https://tel.archives-](https://tel.archives-ouvertes.fr/tel-02496674)  
477 [ouvertes.fr/tel-02496674](https://tel.archives-ouvertes.fr/tel-02496674).
- 478 17. Gradstein, F., and Ogg, J. (1996). Geological time scale for the Phanerozoic.  
479 *Episodes*, 19(1–2):3–6, <https://doi.org/10.18814/epiiugs/1996/v19i1.2/002>.
- 480 18. Granot, R., and Dymant, J. (2019). The influence of post- accretion sedimentation on  
481 marine magnetic anomalies. *Geophysical Research Letters*, 46:4645–4652.  
482 <https://doi.org/10.1029/2019GL082265>.
- 483 19. Hall, D. J., Cavanaugh, T. D., Watkins, J. S., and McMillen, K. J. (1982). The  
484 Rotational Origin of the Gulf of Mexico Based on Regional Gravity Data: Rifted  
485 Margins: Field Investigations of Margin Structure and Stratigraphy. *AAPG memoir*,  
486 34:115-126, <https://doi.org/10.1306/M34430>.

- 487 20. Hall, D. J. (1990). Gulf Coast-East Coast magnetic anomaly I: Root of the main,  
488 crustal decollement for the Appalachian-Ouachita orogen. *Geology*, 18(9):862-865,  
489 [https://doi.org/10.1130/0091-7613\(1990\)018<0862:GCECMA>2.3.CO;2](https://doi.org/10.1130/0091-7613(1990)018<0862:GCECMA>2.3.CO;2).
- 490 21. Kent, D. V., and Gradstein, F. M. (1986). A Jurassic to recent chronology. *The*  
491 *Geology of North America*, 1000:45–50, <https://doi.org/10.1130/DNAG-GNA-M.45>.
- 492 22. Keppie, D. F., and Keppie, J. D. (2014). The Yucatan, a Laurentian or Gondwanan  
493 fragment? Geophysical and palinspastic constraints. *International Journal of Earth*  
494 *Sciences*, 103(5):1501–1512, <https://doi.org/10.1007/s00531-013-0953-x>.
- 495 23. Lesur, V., Hamoudi, M., Choi, Y., Dyment, J., and Thébault, E. (2016). Building the  
496 second version of the World Digital Magnetic Anomaly Map (WDMAM). *Earth,*  
497 *Planets and Space*, 68(1):1–13, <https://doi.org/10.1186/s40623-016-0404-6>.
- 498 24. Levi, S., and Riddihough, R. (1986). Why are marine magnetic anomalies suppressed  
499 over sedimented spreading centers. *Geology*, 14 (8): 651–654.  
500 [https://doi.org/10.1130/0091-7613\(1986\)14<651:WAMMAS>2.0.CO;2](https://doi.org/10.1130/0091-7613(1986)14<651:WAMMAS>2.0.CO;2)
- 501 25. Lin, P., Bird, D.E., and Mann, P. (2019). Crustal structure of an extinct, late Jurassic-  
502 to-earliest Cretaceous spreading center and its adjacent oceanic crust in the eastern  
503 Gulf of Mexico. *Mar Geophys Res*, 40:395–418, [https://doi.org/10.1007/s11001-019-](https://doi.org/10.1007/s11001-019-09379-5)  
504 [09379-5](https://doi.org/10.1007/s11001-019-09379-5).
- 505 26. Lundin, E.R., and Doré, A.G. (2017) The Gulf of Mexico and Canada Basin: Genetic  
506 Siblings on Either Side of North America. *GSA Today*, 27(1):4-11,  
507 <https://doi.org/10.1130/GSATG274A.1>.
- 508 27. Malinverno, A., Hildebrandt, J., Tominaga, M., and Channell, J. E. (2012). M-  
509 sequence geomagnetic polarity time scale (MHTC12) that steadies global spreading  
510 rates and incorporates astrochronology constraints. *Journal of Geophysical Research:*  
511 *Solid Earth*, 117(B6), <https://doi.org/10.1029/2012JB009260>.

- 512 28. Marton, G., and Buffler, R. T. (1994). Jurassic reconstruction of the Gulf of Mexico  
513 Basin. *International Geology Review*, 36(6):545–586,  
514 <https://doi.org/10.1080/00206819409465475>.
- 515 29. Marton, G., and Buffler, R. T. (2016). Jurassic-Cretaceous Tectonic Evolution of the  
516 Southeastern Gulf of Mexico, Constrains on the Style and Timing of Gulf of Mexico  
517 Rift-Drift Development, #41945, in AAPG/SEG International Conference &  
518 Exhibition, Cancun, Mexico, September 6-9, 2016.
- 519 30. Marzoli, A., Renne, P. R., Piccirillo, E. M., Ernesto, M., Bellieni, G., and De Min, A.  
520 (1999). Extensive 200-million-year-old continental flood basalts of the Central  
521 Atlantic Magmatic Province. *Science*, 284(5414):616–618,  
522 <https://doi.org/10.1126/science.284.5414.616>.
- 523 31. Minguetz, D., Gerald Hensel, E., Johnson, E. (2020). A fresh look at Gulf of Mexico  
524 tectonics: Testing rotations and breakup mechanisms from the perspective of  
525 seismically constrained potential-fields modeling and plate kinematics. *Interpretation*,  
526 8:4, SS31-SS45, <https://doi.org/10.1190/INT-2019-0256.1>.
- 527 32. Molina-Garza, R. S., Van Der Voo, R. O. B., and Urrutia-Fucugauchi, J. (1992).  
528 Paleomagnetism of the Chiapas Massif, southern Mexico: Evidence for rotation of the  
529 Maya Block and implications for the opening of the Gulf of Mexico. *Geological  
530 Society of America Bulletin*, 104(9):1156-1168, [https://doi.org/10.1130/0016-  
531 7606\(1992\)104<1156:POTCMS>2.3.CO;2](https://doi.org/10.1130/0016-7606(1992)104<1156:POTCMS>2.3.CO;2).
- 532 33. Nguyen, L., and Mann, P. (2015). Gravity and magnetic constraints on the Jurassic  
533 opening of the oceanic Gulf of Mexico and the location and tectonic history of the  
534 Western Main transform fault along the eastern continental margin of Mexico.  
535 *Interpretation*, 4(1), SC23-SC33, <https://doi.org/10.1190/INT-2015-0110.1>.

- 536 34. Pindell, J. and Dewey, J. F. (1982). Permo-Triassic reconstruction of western Pangea  
537 and the evolution of the Gulf of Mexico/Caribbean region. *Tectonics*, 1(2):179–211,  
538 <https://doi.org/10.1029/TC001i002p00179>.
- 539 35. Pindell, J. L. (1985). Alleghenian reconstruction and subsequent evolution of the Gulf  
540 of Mexico, Bahamas, and proto-Caribbean. *Tectonics*, 4(1):1–39,  
541 <https://doi.org/10.1029/TC004i001p00001>.
- 542 36. Pindell, J., Miranda, C., Ceron, A., and Hernandez, L. (2016). Aeromagnetic map  
543 constrains Jurassic–Early Cretaceous synrift, break up, and rotational seafloor  
544 spreading history in the Gulf of Mexico. In *Mesozoic of the Gulf Rim and Beyond:*  
545 *New Progress in Science and Exploration of the Gulf of Mexico Basin. 35th Annual*  
546 *Gulf Coast Section SEPM Foundation Perkins-Rosen Research Conference, GCS*  
547 *SEPM Foundation, Houston, TX, USA, 123–153,*  
548 <https://doi.org/10.5724/gcs.15.35.0123>.
- 549 37. Pindell, J., Villagómez, D., Molina-Garza, R., Graham, R. and Weber, B. (2020). A  
550 revised synthesis of the rift and drift history of the Gulf of Mexico and surrounding  
551 regions in the light of improved age dating of the Middle Jurassic salt. *Geological*  
552 *Society, London, Special Publications, 504:29-76, 1 October 2020,*  
553 <https://doi.org/10.1144/SP504-2020-43>.
- 554 38. Ross, M. I., and Scotese, C. R. (1988). A hierarchical tectonic model of the Gulf of  
555 Mexico and Caribbean region. *Tectonophysics*, 155(1-4):139–168,  
556 [https://doi.org/10.1016/0040-1951\(88\)90263-6](https://doi.org/10.1016/0040-1951(88)90263-6).
- 557 39. Sabaka, T., Olsen, N., and Purucker, M. E. (2004) Extending comprehensive models  
558 of the Earth's magnetic field with Ørsted and CHAMP data. *Geophysical Journal*  
559 *International*, 159(2):521–547, <https://doi.org/10.1111/j.1365-246X.2004.02421.x>.

- 560 40. Sandwell, D. T., Müller, R. D., Smith, W. H., Garcia, E., and Francis, R. (2014). New  
561 global marine gravity model from CryoSat-2 and Jason-1 reveals buried tectonic  
562 structure. *Science*, 346(6205):65-67, <https://doi.org/science.1258213>.
- 563 41. Schlager, W., Buffler, R. T., Angstadt, D., Bowdler, J. L., COTILLON, P.,  
564 Dallmeyer, R. D., Halley, R. B., Kinoshita, H., Magoon, L. B. III, McNulty, C. L.,  
565 Patton, J. W., Pisciotto, K. A., Premoli-Silva, I., Suarez, O. A., Testarmata, M. M.,  
566 Tyson, R. V., and Watkins, D. K. (1984). Deep Sea Drilling Project Leg 77:  
567 Southeastern Gulf of Mexico. *Geological Society of America Bulletin*, 95:226–236,  
568 [https://doi.org/10.1130/0016-7606\(1984\)95<226:DSDPLS>2.0.CO;2](https://doi.org/10.1130/0016-7606(1984)95<226:DSDPLS>2.0.CO;2).
- 569 42. Schouten, H., and Klitgord, K. D. (1994). Mechanistic solutions to the opening of the  
570 Gulf of Mexico. *Geology*, 22(6):507–510, [https://doi.org/10.1130/0091-7613\(1994\)022<0507:MSTTOO>2.3.CO;2](https://doi.org/10.1130/0091-7613(1994)022<0507:MSTTOO>2.3.CO;2).
- 571
- 572 43. Snedden, J.W., Virdell, J., Whiteaker, T.L., Ganey-Curry, P. (2015) A basin-scale  
573 perspective on Cenomanian-Turonian (Cretaceous) depositional systems, greater Gulf  
574 of Mexico (USA). *Interpretation*, 4(1):SC1–SC22. doi: <https://doi.org/10.1190/INT-2015-0082.1>.
- 575
- 576 44. Stern, R. J., and Dickinson, W. R. (2010) The Gulf of Mexico is a Jurassic backarc  
577 basin, *Geosphere*, 6(6):739-754, <https://doi.org/10.1130/GES00585.1>.
- 578 45. Tominaga, M., and Sager, W. (2010). Revised Pacific M-anomaly geomagnetic  
579 polarity time scale. *Geophysical Journal International*, 182(1):203–232,  
580 <https://doi.org/10.1111/j.1365-246X.2010.04619.x>.
- 581 46. Van Avendonk, H., Christeson, Gail., Norton, I., Eddy, D. (2015) Continental rifting  
582 and sediment infill in the northwestern Gulf of Mexico. *Geology*, 43(7):631–634,  
583 <https://doi.org/10.1130/G367981> .

584 47. van Hinsbergen, D.J.J., de Groot, L.V., van Schaik, S.J., Spakman, W., Bijl, P.K.,  
585 Sluijs, A., Langereis, C.G., Brinkhuis, H. (2015) A Paleolatitude Calculator for  
586 Paleoclimate Studies, PLOS ONE, 10(6), e0126946,  
587 <https://doi.org/10.1371/journal.pone.0126946>.  
588

589 **FIGURE CAPTIONS**

590 **Figure 1.** Potential field maps of the Gulf of Mexico. (a) Original and (b) interpreted  
591 magnetic anomaly (on land: [Lesur et al., 2016](#)); (c) Original and (d) interpreted vertical  
592 gradient of gravity ([Sandwell et al., 2014](#)). Solid black lines, seafloor spreading magnetic  
593 anomalies; solid red lines, fossil spreading axis and isolated segments; blue solid lines,  
594 fracture zones; black dotted lines, continent-ocean boundary (COB). Numbers on land  
595 correspond to magnetic domains: Yucatán (1) and Florida (2) cratonic blocks, the Sierra  
596 Madre mountain range (3) and the basins fringing Louisiana and Texas (4).

597 **Figure 2.** Magnetic anomaly maps of the reconstructed Gulf of Mexico at the time of  
598 A) GoM2o (~150 Ma), B) GoM2y (~147), and C) GoM1y (~140 Ma). The Yucatan Block is  
599 rotated with respect to fixed North America. Thick color line marks the spreading center, and  
600 colored star the Euler pole of the corresponding finite rotation. Color circles are constraining  
601 points for plate reconstructions. The dashed line delineates the Yucatan Block before rotation.  
602 The thick black line displays the continental part of Yucatan Block. Grey and black thin lines  
603 represent the initial and rotated coastlines, respectively.

604 **Figure 3.** Tectonic model for the evolution of the Gulf of Mexico. Solid black lines, seafloor  
605 spreading magnetic anomalies labeled in red; solid red lines, fossil spreading axis and  
606 isolated segments; blue solid lines, fracture zones; dotted black lines, continent-ocean  
607 boundary (COB); color circles, constraining points for plate reconstructions; color stars,  
608 Euler poles for finite (black contours, labelled F) and stage (no contour, labelled S) rotations.  
609 Purple, COB pseudo-reconstruction; Blue and green, GoM2o-GoM2y and GoM2y-GoM1y  
610 reconstructions. Blue and green lines represent computed flowlines for the corresponding  
611 periods. Background colors show the vertical gradient of gravity (see Figure 1c).

612 **Figure 4.** Dating intermediate wavelength magnetic anomalies in the Gulf of Mexico. A)  
613 Filtered geomagnetic polarity time scale ([Malinverno et al., 2012](#)) with, black line, original

614 GPTS; blue and green lines, low-pass filtered GPTS retaining wavelengths higher than 3 Myr  
615 and 5 Myr, respectively. The GPTS has been inverted to take into account the configuration  
616 of the Gulf of Mexico at the time of its opening. The red square marks the proposed  
617 identification. B) Magnetic anomaly profiles extracted from the magnetic anomaly map of the  
618 Gulf of Mexico (background) along five selected flowlines. The corresponding anomalies are  
619 projected perpendicular to each profile, with different colors for clarity. C) Magnetic anomaly  
620 profiles (red lines) and filtered GPTS (blue and green lines filtered as in A) showing the  
621 proposed magnetic interpretation. Dark and light shades mark GoM1 and GoM2 anomalies,  
622 respectively. Dotted black lines mark the fossil spreading axis and possible other fossil  
623 spreading segments suggested by the vertical gradient of gravity.  
624

Garcia-Reyes and Dyment, Figure 1

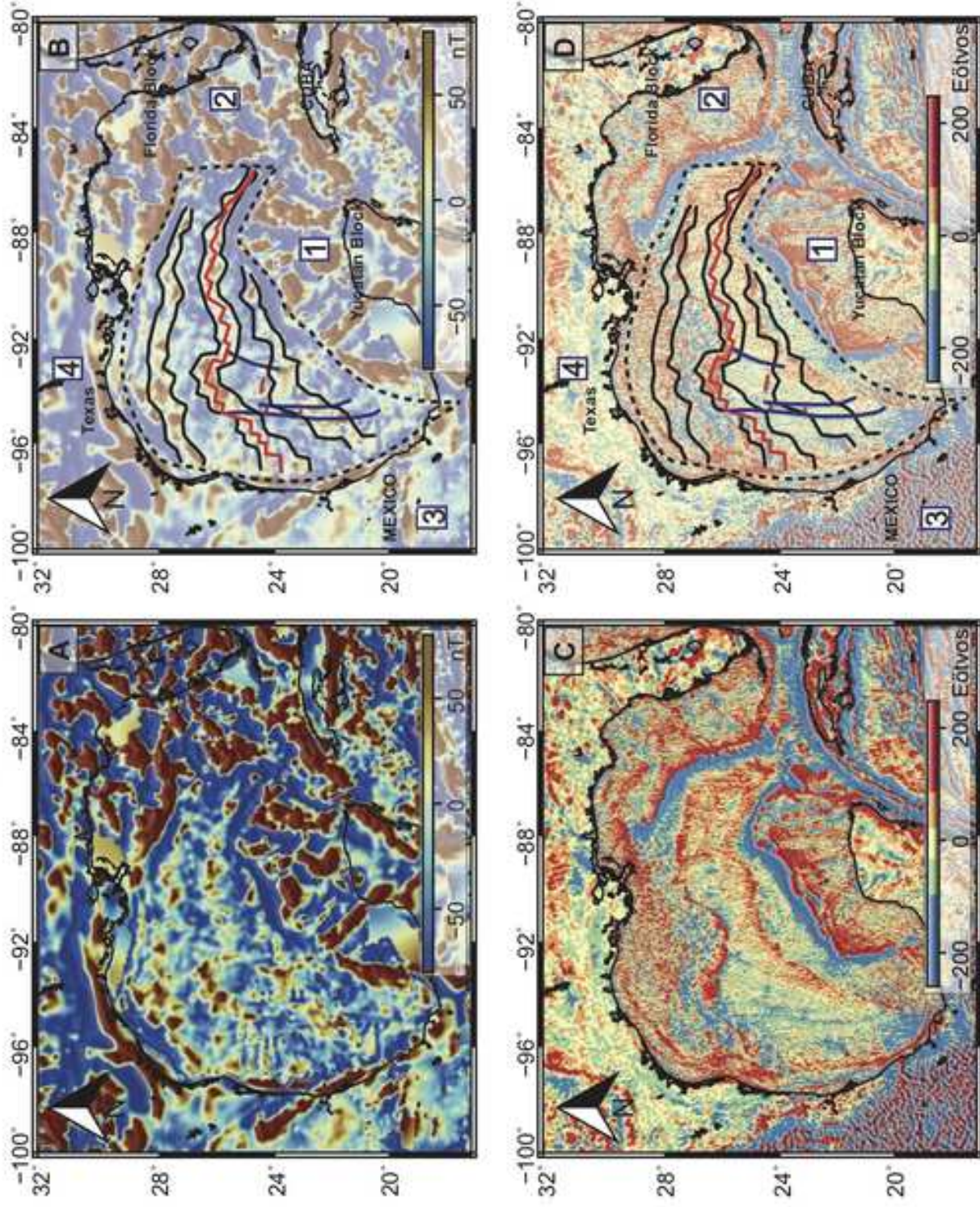
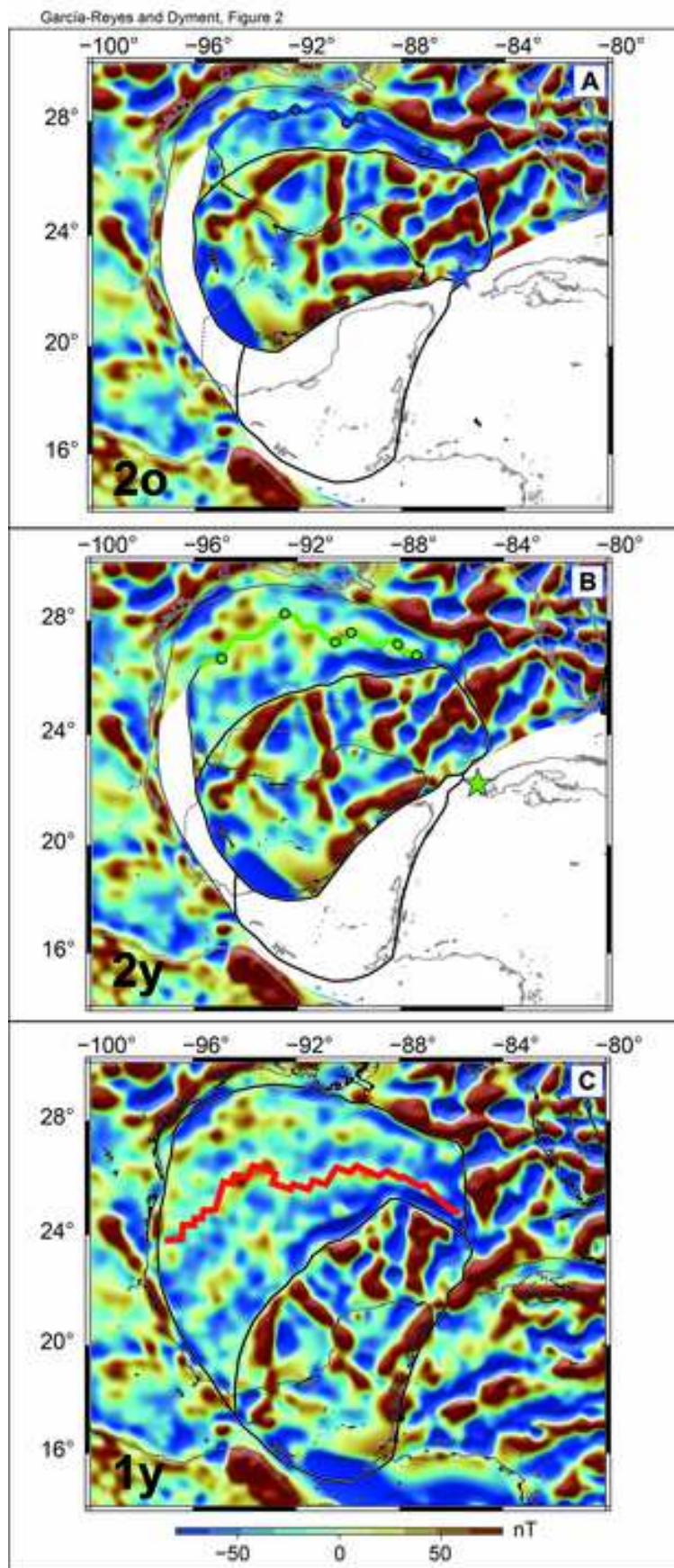
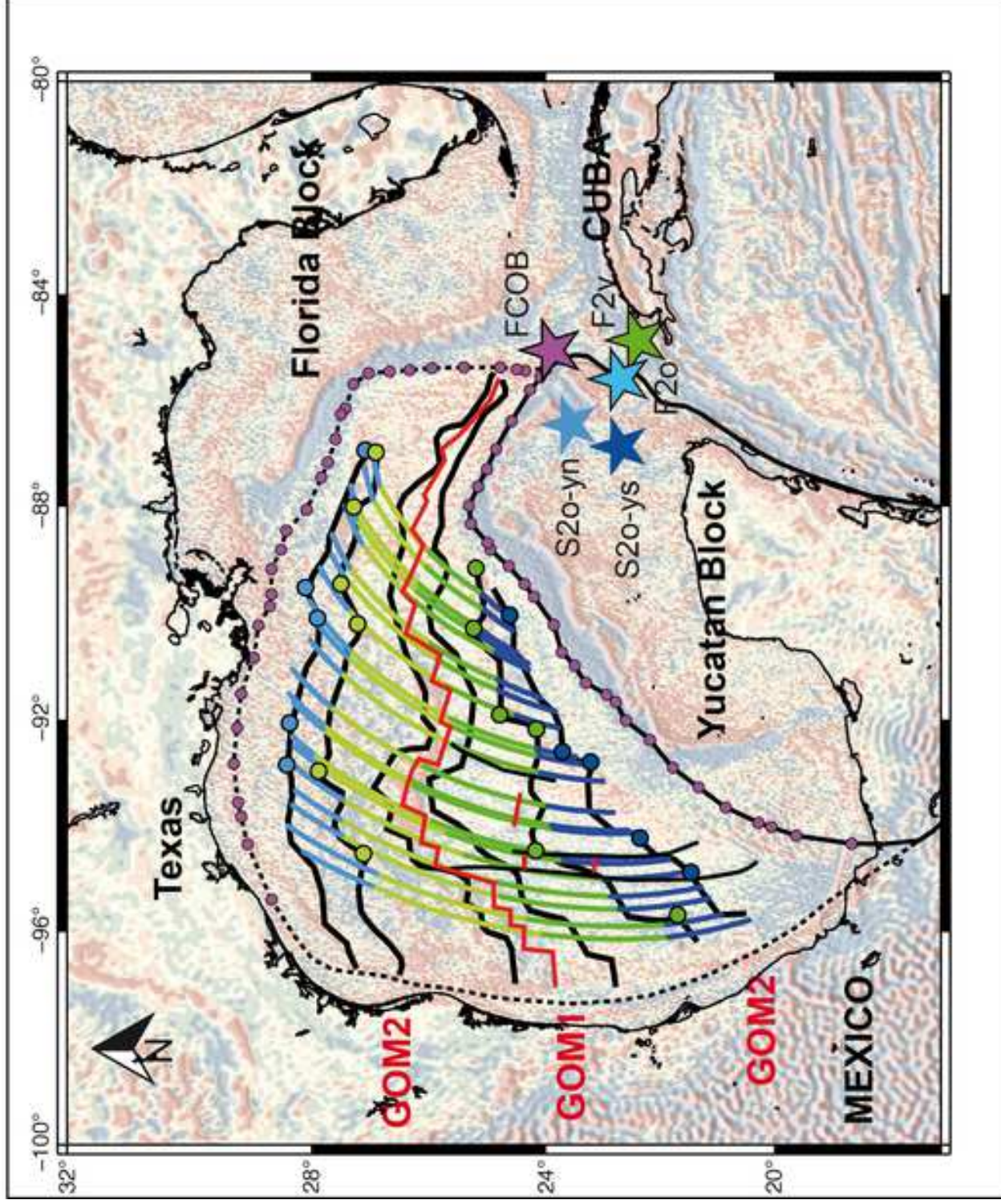


Figure 2

[Click here to access/download;Figure;Figure\\_2\\_Garcia\\_Dyment\\_R1.jpg](#)



Garcia and Dyment, Figure 3



Garcia-Reyes and Dyment, Figure 4

